

Estimating temporally variable selection intensity from ancient DNA data with the flexibility of modelling linkage and epistasis

Zhangyi He^{a,1,*}, Xiaoyang Dai^{b,1}, Wenyang Lyu^c, Mark Beaumont^d, Feng Yu^c

^a*Cancer Research UK Beatson Institute, Glasgow G61 1BD, United Kingdom*

^b*The Blizard Institute, Barts and The London School of Medicine and Dentistry, Queen Mary University of London, London E1 2AT, United Kingdom*

^c*School of Mathematics, University of Bristol, Bristol BS8 1UG, United Kingdom*

^d*School of Biological Sciences, University of Bristol, Bristol BS8 1TQ, United Kingdom*

Abstract

Innovations in ancient DNA (aDNA) preparation and sequencing technologies have exponentially increased the quality and quantity of aDNA data extracted from ancient biological materials. The additional temporal component from the incoming aDNA data can provide improved power to address fundamental evolutionary questions like characterising selection processes that shape the phenotypes and genotypes of contemporary populations or species. However, utilising aDNA to study past selection processes still involves considerable hurdles such as how to eliminate the confounding effect of genetic interactions in the inference of selection. To circumvent this challenge, in this work we extend the method introduced by He et al. (2022) to infer temporally variable selection from the data on aDNA sequences with the flexibility of modelling linkage and epistasis. Our posterior computation is carried out through a robust adaptive version of the particle marginal Metropolis-Hastings algorithm with a coerced acceptance rate. Moreover, our extension inherits their desirable features like modelling sample uncertainties resulting from the damage and fragmentation of aDNA molecules and reconstructing underlying gamete frequency trajectories of the population. We assess the performance and show the utility of our procedure with an application to ancient horse samples genotyped at the loci encoding base coat colours and pinto coat patterns.

Keywords: Ancient DNA, Natural selection, Genetic linkage, Epistatic interaction, Two-layer hidden Markov model, Adaptive particle marginal Metropolis-Hastings

*Corresponding author.

Email address: z.he@beatson.gla.ac.uk (Zhangyi He)

¹These authors contributed equally to this work.

1. Introduction

Natural selection is one of the primary mechanisms of evolutionary changes and is responsible for the evolution of adaptive features (Darwin, 1859). A full understanding of the role of selection in driving evolutionary changes needs accurate estimates of the underlying timing and strength of selection. With recent advances in sequencing technologies and molecular techniques tailored to ultra-damaged templates, high-quality time serial samples of segregating alleles have become increasingly common in ancestral populations, (*e.g.*, Ludwig et al., 2009; Mathieson et al., 2015; Allentoft et al., 2015; Ramos-Madrigal et al., 2016; Loog et al., 2017; Librado et al., 2017; Fages et al., 2019; Alves et al., 2019). The additional temporal dimension of the ancient DNA (aDNA) data has the promise of boosting power for the estimation of population genetic parameters, in particular for the pace of adaptation, as the allele frequency trajectory through time itself gives us valuable information collected before, during and after genetic changes driven by selection. See Dehasque et al. (2020) for a detailed review of the inference of selection from aDNA.

The temporal component provided by the incoming aDNA data spurred the development of statistical approaches for the inference of selection from time series data of allele frequencies in the last fifteen years (see Malaspinas, 2016, for a detailed review). Most existing approaches are built upon the hidden Markov model (HMM) framework of Williamson & Slatkin (1999), where the population allele frequency is modelled as a hidden state evolving under the Wright-Fisher model (Fisher, 1922; Wright, 1931), and the sample allele frequency drawn from the underlying population at each given time point is modelled as a noisy observation of the population allele frequency (see Tataru et al., 2017, for an excellent review of statistical inference in the Wright-Fisher model based on time series data of allele frequencies). However, such an HMM framework can be computationally infeasible for large population sizes and evolutionary timescales owing to a prohibitively large amount of computation and storage required in its likelihood calculations.

To our knowledge, most existing methods tailored to aDNA rely on the diffusion approximation of the Wright-Fisher model. By working with the diffusion approximation, its HMM framework permits efficient integration over the probability distribution of the underlying population allele frequencies and therefore the calculation of the likelihood based on the observed sample allele frequencies can be completed within a reasonable amount of time (*e.g.*, Bollback et al., 2008; Malaspinas et al., 2012; Steinrücken et al., 2014; Schraiber et al., 2016; Ferrer-Admetlla

31 et al., 2016; He et al., 2020b,c; Lyu et al., 2022; He et al., 2022). These approaches have already
32 been successfully used in aDNA studies; *e.g.*, the method of Bollback et al. (2008) was applied
33 in Ludwig et al. (2009) to analyse the aDNA data associated with horse coat colouration and
34 illustrated that positive selection acted on the derived *ASIP* and *MC1R* alleles, suggesting that
35 domestication and selective breeding contributed to changes in horse coat colouration.

36 Despite the availability of a certain number of statistical methods for the inference of selec-
37 tion from genetic time series, their application to aDNA data from natural populations remains
38 limited. Most existing methods were developed in the absence of genetic interactions like linkage
39 and epistasis, with the exception of *e.g.*, He et al. (2020b). In He et al. (2020b), local linkage
40 and genetic recombination were explicitly modelled, which has been demonstrated to contribute
41 to significant improvements in the inference of selection, in particular for tightly linked loci. Ig-
42 noring epistasis can also cause severe issues in the study of selection since the combined effects
43 of mutant alleles may be impossible to predict according to the measured individual effects of a
44 given mutant allele (Bank et al., 2014). As an example, horse base coat colours (*i.e.*, bay, black
45 and chestnut) are primarily determined by *ASIP* and *MC1R*, and the derived *ASIP* and *MC1R*
46 alleles have been shown to be selectively advantageous with ancient horse samples through ex-
47 isting approaches (*e.g.*, Bollback et al., 2008; Malaspinas et al., 2012; Steinrücken et al., 2014;
48 Schraiber et al., 2016; He et al., 2020c). However, this is not sufficient enough to conclude that
49 black horses were favoured by selection as alleles at *MC1R* interact epistatically with those at
50 *ASIP*, *i.e.*, the presence of at least one copy of the dominant ancestral allele at *MC1R*, and the
51 resulting production of black pigment, is required to check the action of alleles at *ASIP* (Corbin
52 et al., 2020).

53 To circumvent this issue, in this work we introduce a novel Bayesian method for the inference
54 of selection acting on the phenotypic trait, allowing the intensity to vary over time, from data on
55 aDNA sequences, with the flexibility of modelling genetic linkage and epistatic interaction. Our
56 method is built upon the two-layer HMM framework of He et al. (2022), and our key innovation
57 is to introduce a Wright-Fisher diffusion that can model the dynamics of two linked genes under
58 phenotypic selection over time to be the underlying Markov process, which permits linkage and
59 epistasis. To remain computationally feasible, our posterior computation is carried out with the
60 particle marginal Metropolis-Hastings (PMMH) algorithm introduced by Andrieu et al. (2010),

61 where we adopt the adaptation strategy proposed by Vihola (2012) to tune the covariance structure
62 of the proposal to achieve a given acceptance rate. Also, our approach inherits certain desirable
63 features from He et al. (2022) like modelling sample uncertainties resulting from the damage
64 and fragmentation of aDNA molecules and reconstructing underlying frequency trajectories of
65 the gametes in the population.

66 We reanalyse the aDNA data associated with horse base coat colours and pinto coat patterns
67 from Wutke et al. (2016) to show the applicability of our method on aDNA data, where base coat
68 colours (bay, black and chestnut) are controlled by the *ASIP* and *MC1R* genes with epistatic
69 interaction while pinto coat patterns (solid, sabino and tobiano) are determined by the *KIT13*
70 and *KIT16* genes with tight linkage. We compare our results with those produced through the
71 approach of He et al. (2022) to demonstrate the necessity of modelling linkage and epistasis in the
72 inference of selection. We test our approach with extensive simulations for each phenotypic trait
73 to show that our procedure can deliver accurate selection inferences from genotype likelihoods.

74 2. Materials and Methods

75 In this section, we construct a Wright-Fisher model to characterise two linked genes evolving
76 under phenotypic selection over time first and then derive its diffusion limit. Working with the
77 diffusion approximation, we extend the approach of He et al. (2022) to infer temporally variable
78 selection from the data on aDNA sequences while modelling linkage and epistasis.

79 2.1. Wright-Fisher diffusion

80 We consider a population of randomly mating diploid individuals represented by alleles at
81 loci \mathcal{A} and \mathcal{B} evolving under selection with discrete non-overlapping generations. At each locus,
82 there are two possible allele types, labelled \mathcal{A}_0 , \mathcal{A}_1 and \mathcal{B}_0 , \mathcal{B}_1 , respectively, resulting in four
83 possible haplotypes on both loci, $\mathcal{A}_0\mathcal{B}_0$, $\mathcal{A}_0\mathcal{B}_1$, $\mathcal{A}_1\mathcal{B}_0$ and $\mathcal{A}_1\mathcal{B}_1$, labelled haplotypes 00, 01, 10
84 and 11, respectively. We attach the symbols \mathcal{A}_0 and \mathcal{B}_0 to the ancestral alleles, which we assume
85 originally exist in the population, and we attach the symbols \mathcal{A}_1 and \mathcal{B}_1 to the mutant alleles,
86 which we assume arise only once in the population. Given the absence of sex effects, this setup
87 gives rise to 10 possible (unordered) genotypes $\mathcal{A}_i\mathcal{B}_j/\mathcal{A}_{i'}\mathcal{B}_{j'}$, which correspond to at most 10
88 distinct phenotypes $\mathcal{P}_{ij,i'j'}$. Phenotypes $\mathcal{P}_{ij,i'j'}$ and $\mathcal{P}_{i'j',ij}$ are identical in our notation.

89 We incorporate viability selection into the population dynamics and assume that the viability
 90 is only determined by the phenotype. Viabilities of all genotypes at loci \mathcal{A} and \mathcal{B} per generation
 91 are assigned $1 + s_{ij,i'j'}$, where $s_{ij,i'j'}$ is the selection coefficient of the $\mathcal{P}_{ij,i'j'}$ phenotype with
 92 $s_{ij,i'j'} \in [-1, +\infty)$ and $s_{ij,i'j'} = s_{i'j',ij}$. In what follows, we let the selection coefficient $s_{00,00} = 0$
 93 unless otherwise noted, and then $s_{ij,i'j'}$ denotes the selection coefficient of the $\mathcal{P}_{ij,i'j'}$ phenotype
 94 against the $\mathcal{P}_{00,00}$ phenotype.

95 2.1.1. Wright-Fisher model

96 Let $X_{ij}^{(N)}(k)$ denote the gamete frequency of haplotype ij at generation $k \in \mathbb{N}$ and $\mathbf{X}^{(N)}(k)$
 97 be the vector of the four gamete frequencies. To incorporate non-constant demographic histories,
 98 we assume that the population size changes deterministically, with $N(k)$ denoting the number
 99 of diploid individuals in the population at generation k . In the Wright-Fisher model, we assume
 100 that gametes are randomly chosen from an effectively infinite gamete pool reflecting the parental
 101 gamete frequencies at each generation. We therefore have

$$\mathbf{X}^{(N)}(k+1) \mid \mathbf{X}^{(N)}(k) = \mathbf{x} \sim \frac{1}{2N(k)} \text{Multinomial}(2N(k), \mathbf{p}), \quad (1)$$

102 where \mathbf{p} is the vector of parental gamete frequencies. Under the assumption of random mating,
 103 we can further express the vector of parental gamete frequencies as

$$p_{ij} = (1-r)x'_{ij} + r \left(\sum_{j=0}^1 x'_{ij} \right) \left(\sum_{i=0}^1 x'_{ij} \right) \quad (2)$$

104 for $i, j \in \{0, 1\}$, where

$$x'_{ij} = \frac{\sum_{i',j'=0}^1 (1 + s_{ij,i'j'}) x_{i'j'} x_{ij}}{\sum_{i,j=0}^1 \sum_{i',j'=0}^1 (1 + s_{ij,i'j'}) x_{i'j'} x_{ij}}, \quad (3)$$

105 and r denotes the recombination rate of the \mathcal{A} and \mathcal{B} loci located on the same chromosome, *i.e.*,
 106 the fraction of recombinant offspring showing a crossover between the two loci per generation. If
 107 the \mathcal{A} and \mathcal{B} loci are located on separate chromosomes, we let the (artificial) recombination rate
 108 $r = 0.5$ (*i.e.*, free recombination). The two-locus Wright-Fisher model with selection is defined
 109 as the Markov process $\mathbf{X}^{(N)}$ evolving with transition probabilities in Eq. (1) in the state space
 110 $\Omega_{\mathbf{X}^{(N)}} = \{\mathbf{x} \in \{0, 1/(2N), \dots, 1\}^4 : \sum_{i,j=0}^1 x_{ij} = 1\}$.

111 *2.1.2. Diffusion approximation*

112 We study the two-locus Wright-Fisher model with selection through its diffusion limit due
 113 to the complicated nature of its transition probability matrix, in particular for large population
 114 sizes or evolutionary timescales. More specifically, we measure time in a unit of $2N_0$ generations,
 115 denoted by t , where N_0 is an arbitrary reference population size fixed through time, and assume
 116 that the selection coefficients and recombination rate are all of order $1/(2N_0)$. As the reference
 117 population size N_0 approaches infinity, the scaled selection coefficients $\alpha_{ij,i'j'} = 2N_0 s_{ij,i'j'}$ and
 118 the scaled recombination rate $\rho = 4N_0 r$ are kept constant, and the ratio of the population size
 119 to the reference population size $N(t)/N_0$ converges to a function, denoted by $\beta(t)$. Notice that
 120 the assumption will be violated if the \mathcal{A} and \mathcal{B} loci are located on separate chromosomes, *i.e.*,
 121 $r = 0.5$, but we shall nevertheless use this scaling to find the drift term in the diffusion limit. We
 122 will plug the unscaled recombination rate r into the resulting system of stochastic differential
 123 equations (SDE's) and use that as our diffusion approximation.

124 Let $\Delta X_{ij}^{(N)}(k)$ denote the change in the gamete frequency of haplotype ij over generation k .
 125 With standard techniques of diffusion theory (see, *e.g.*, Karlin & Taylor, 1981), we can formulate
 126 the infinitesimal mean vector $\boldsymbol{\mu}(t, \mathbf{x})$ and the infinitesimal (co)variance matrix $\boldsymbol{\Sigma}(t, \mathbf{x})$ as

$$\begin{aligned} \mu_{ij}(t, \mathbf{x}) &= \lim_{N_0 \rightarrow \infty} 2N_0 \mathbb{E}[\Delta X_{ij}^{(N)}([2N_0 t]) \mid \mathbf{X}^{(N)}([2N_0 t]) = \mathbf{x}] \\ &= \lim_{N_0 \rightarrow \infty} 2N_0(p_{ij} - x_{ij}) \end{aligned} \quad (4)$$

$$\begin{aligned} \Sigma_{ij,i'j'}(t, \mathbf{x}) &= \lim_{N_0 \rightarrow \infty} 2N_0 \mathbb{E}[\Delta X_{ij}^{(N)}([2N_0 t]) \Delta X_{i'j'}^{(N)}([2N_0 t]) \mid \mathbf{X}^{(N)}([2N_0 t]) = \mathbf{x}] \\ &= \lim_{N_0 \rightarrow \infty} \frac{2N_0}{2N([2N_0 t])} p_{ij} (\delta_{ii'} \delta_{jj'} - p_{i'j'}) + 2N_0 (p_{ij} - x_{ij})(p_{i'j'} - x_{i'j'}) \end{aligned} \quad (5)$$

127 for $i, j, i', j' \in \{0, 1\}$, where δ denotes the Kronecker delta function and $[\cdot]$ is used to represent
 128 the integer part of the value in the brackets.

129 To obtain the expression for the infinitesimal mean vector $\boldsymbol{\mu}(t, \mathbf{x})$, we compute the limit of
 130 the expected change in the gamete frequency of haplotype ij within a single generation as the
 131 reference population size N_0 goes to infinity. The only terms that survive after taking the limit
 132 are the first order terms in the Taylor expansion of the sampling probability p_{ij} in Eq. (2) with
 133 respect to the selection coefficients $s_{ij,i'j'}$ and the recombination rate r . The infinitesimal mean

134 vector $\boldsymbol{\mu}(t, \boldsymbol{x})$ can then be written down as

$$\mu_{ij}(t, \boldsymbol{x}) = x_{ij} \sum_{i',j'=0}^1 \alpha_{ij,i'j'} x_{i'j'} - x_{ij} \sum_{i',j'=0}^1 \sum_{i,j=0}^1 x_{ij} \alpha_{ij,i'j'} x_{i'j'} - (-1)^{\delta_{ij}} \frac{\rho}{2} (x_{00}x_{11} - x_{01}x_{10}) \quad (6)$$

135 for $i, j \in \{0, 1\}$. Note that we take the scaled recombination rate to be $\rho = 2N_0$ (*i.e.*, the (ar-
136 tificial) recombination rate $r = 0.5$) if the \mathcal{A} and \mathcal{B} loci are located on separate chromosomes.
137 Such a strong recombination term serves to uncouple the two genes located on separate chromo-
138 somes. The infinitesimal (co)variance matrix $\boldsymbol{\Sigma}(t, \boldsymbol{x})$ corresponds to the standard Wright-Fisher
139 diffusion on four haplotypes (see, *e.g.*, He et al., 2020a). That is, we have

$$\Sigma_{ij,i'j'}(t, \boldsymbol{x}) = \frac{x_{ij}(\delta_{ii'}\delta_{jj'} - x_{i'j'})}{\beta(t)} \quad (7)$$

140 for $i, j, i', j' \in \{0, 1\}$.

141 Combining the Wright-Fisher diffusion with the infinitesimal mean vector $\boldsymbol{\mu}(t, \boldsymbol{x})$ in Eq. (6)
142 and the infinitesimal (co)variance matrix $\boldsymbol{\Sigma}(t, \boldsymbol{x})$ in Eq. (7), we achieve the following system of
143 SDE's as our diffusion approximation of the Wright-Fisher model in Eq. (1)

$$dX_{ij}(t) = \mu_{ij}(t, \boldsymbol{X}(t))dt + \sum_{i',j'=0}^1 \sqrt{\frac{X_{ij}(t)X_{i'j'}(t)}{\beta(t)}} dW_{ij,i'j'}(t) \quad (8)$$

144 for $i, j \in \{0, 1\}$, where $W_{ij,i'j'}$ denotes an independent standard Wiener process with $W_{ij,i'j'}(t) =$
145 $-W_{i'j',ij}(t)$. This anti-symmetry requirement implies $W_{ij,ij}(t) = 0$, and the (co)variance matrix
146 for the X_{ij} 's is exactly the infinitesimal (co)variance matrix $\boldsymbol{\Sigma}(t, \boldsymbol{x})$ in Eq. (7). We refer to the
147 diffusion process \boldsymbol{X} evolving in the state space $\Omega_{\boldsymbol{X}} = \{\boldsymbol{x} \in [0, 1]^4 : \sum_{i,j=0}^1 x_{ij} = 1\}$ that solves
148 the system of SDE's in Eq. (8) as the two-locus Wright-Fisher diffusion with selection.

149 2.2. Bayesian inference of selection

150 Suppose that the available data are always sampled from the underlying population at a finite
151 number of distinct time points, say $t_1 < t_2 < \dots < t_K$, measured in units of $2N_0$ generations.
152 We assume that N_k individuals are drawn from the underlying population at the k -th sampling
153 time point, and for individual n , let $\boldsymbol{r}_{l,n,k}$ be, in this generic notation, all of the reads at locus
154 l for $l \in \{1, 2\}$. The population genetic quantities of our interest are the selection coefficients
155 $s_{ij,i'j'}$ for $i, j, i', j' \in \{0, 1\}$. Recall that our setup described in Section 2.1.1 gives rise to at most

156 10 distinct phenotypes (*i.e.*, at most 9 distinct selection coefficients). For simplicity, we use $\boldsymbol{\vartheta}$
 157 to represent all distinct selection coefficients to estimate in this work.

158 2.2.1. Hidden Markov model

159 We extend the two-layer HMM framework introduced by He et al. (2022) to model genetic
 160 linkage and epistatic interaction, where the first hidden layer $\mathbf{X}(t)$ characterises the gamete fre-
 161 quency trajectories of the underlying population over time through the Wright-Fisher diffusion
 162 in Eq. (8), the second hidden layer $\mathbf{G}(t)$ represents the genotype of the individual in the sample,
 163 and the third observed layer $\mathbf{R}(t)$ denotes the data on ancient DNA sequences. See Figure 1 for
 164 the graphical representation of our HMM framework for the data on ancient DNA sequences.

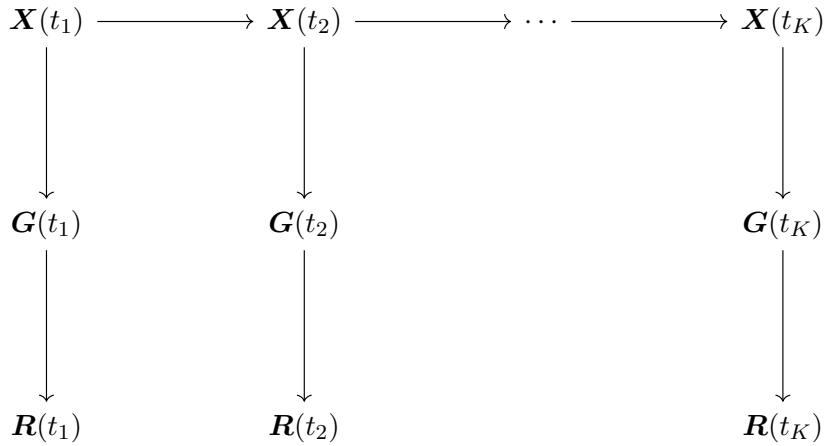


Figure 1: Graphical representation of the two-layer HMM framework extended from He et al. (2022) for the data on ancient DNA sequences.

165 We let $\mathbf{x}_{1:K} = \{\mathbf{x}_1, \mathbf{x}_2, \dots, \mathbf{x}_K\}$ be the frequency trajectories of the gametes in the underly-
 166 ing population at the sampling time points $\mathbf{t}_{1:K}$ and $\mathbf{g}_{1:K} = \{\mathbf{g}_1, \mathbf{g}_2, \dots, \mathbf{g}_K\}$ be the genotypes of
 167 the individuals drawn from the underlying population at the sampling time points $\mathbf{t}_{1:K}$, where
 168 $\mathbf{g}_k = \{\mathbf{g}_{1,k}, \mathbf{g}_{2,k}, \dots, \mathbf{g}_{N_k,k}\}$ and $\mathbf{g}_{n,k} = \{g_{1,n,k}, g_{2,n,k}\}$ with $g_{l,n,k} \in \{0, 1, 2\}$ being the number of
 169 mutant alleles at locus l in individual n at sampling time point t_k . Based on the HMM frame-
 170 work illustrated in Figure 1, the posterior probability distribution for the selection coefficients
 171 and population gamete frequency trajectories can be expressed as

$$p(\boldsymbol{\vartheta}, \mathbf{x}_{1:K} \mid \mathbf{r}_{1:K}) = \sum_{\mathbf{g}_{1:K}} p(\boldsymbol{\vartheta}, \mathbf{x}_{1:K}, \mathbf{g}_{1:K} \mid \mathbf{r}_{1:K}), \quad (9)$$

172 where

$$p(\boldsymbol{\vartheta}, \mathbf{x}_{1:K}, \mathbf{g}_{1:K} \mid \mathbf{r}_{1:K}) \propto p(\boldsymbol{\vartheta})p(\mathbf{x}_{1:K} \mid \boldsymbol{\vartheta})p(\mathbf{g}_{1:K} \mid \mathbf{x}_{1:K})p(\mathbf{r}_{1:K} \mid \mathbf{g}_{1:K}) \quad (10)$$

173 and $\mathbf{r}_{1:K} = \{\mathbf{r}_1, \mathbf{r}_2, \dots, \mathbf{r}_K\}$ with $\mathbf{r}_k = \{\mathbf{r}_{1,k}, \mathbf{r}_{2,k}, \dots, \mathbf{r}_{N_k,k}\}$ and $\mathbf{r}_{n,k} = \{\mathbf{r}_{1,n,k}, \mathbf{r}_{2,n,k}\}$.

174 The first term of the product in Eq. (10), $p(\boldsymbol{\vartheta})$, is the prior probability distribution for the
175 selection coefficients. We can adopt a uniform prior over the interval $[-1, +\infty)$ for each selection
176 coefficient if our prior knowledge is poor.

177 The second term of the product in Eq. (10), $p(\mathbf{x}_{1:K} \mid \boldsymbol{\vartheta})$, is the probability distribution for
178 the population gamete frequency trajectories at all sampling time points. As the Wright-Fisher
179 diffusion is a Markov process, we can decompose the probability distribution $p(\mathbf{x}_{1:K} \mid \boldsymbol{\vartheta})$ as

$$p(\mathbf{x}_{1:K} \mid \boldsymbol{\vartheta}) = p(\mathbf{x}_1 \mid \boldsymbol{\vartheta}) \prod_{k=1}^{K-1} p(\mathbf{x}_{k+1} \mid \mathbf{x}_k; \boldsymbol{\vartheta}), \quad (11)$$

180 where $p(\mathbf{x}_1 \mid \boldsymbol{\vartheta})$ is the prior probability distribution for the population gamete frequencies at the
181 initial sampling time point, set to be a flat Dirichlet distribution over the state space $\Omega_{\mathbf{X}}$ if our
182 prior knowledge is poor, and $p(\mathbf{x}_{k+1} \mid \mathbf{x}_k; \boldsymbol{\vartheta})$ is the transition probability density function of the
183 Wright-Fisher diffusion \mathbf{X} between two consecutive sampling time points for $k = 1, 2, \dots, K-1$,
184 solving the Kolmogorov backward equation (or its adjoint) associated with the Wright-Fisher
185 diffusion in Eq. (8).

186 The third term of the product in Eq. (10), $p(\mathbf{g}_{1:K} \mid \mathbf{x}_{1:K})$, is the probability distribution for
187 the genotypes of all individuals in the sample given the population gamete frequency trajectories
188 at all sampling time points. With the conditional independence from our HMM framework (see
189 Figure 1), we can decompose the probability distribution $p(\mathbf{g}_{1:K} \mid \mathbf{x}_{1:K})$ as

$$p(\mathbf{g}_{1:K} \mid \mathbf{x}_{1:K}) = \prod_{k=1}^K p(\mathbf{g}_k \mid \mathbf{x}_k) = \prod_{k=1}^K \prod_{n=1}^{N_k} p(\mathbf{g}_{n,k} \mid \mathbf{x}_k), \quad (12)$$

190 where $p(\mathbf{g}_{n,k} \mid \mathbf{x}_k)$ is the probability distribution for the genotypes $\mathbf{g}_{n,k}$ of sampled individual n
191 given the gamete frequencies \mathbf{x}_k of the population. Under the assumption that all individuals
192 in the sample are drawn from the population in their adulthood (*i.e.*, the stage after selection
193 but before recombination in the life cycle, see He et al. (2017)), the probability of observing the
194 sampled individual genotypes $\mathbf{g}_{n,k} = (i + i', j + j')$ given the population gamete frequencies \mathbf{x}_k

195 can be calculated with

$$p(\mathbf{g}_{n,k} | \mathbf{x}_k) = \begin{cases} \frac{(1 + s_{ij,i'j'})x_{i'j',k}x_{ij,k}}{\sum_{i,j=0}^1 \sum_{i',j'=0}^1 (1 + s_{ij,i'j'})x_{i'j',k}x_{ij,k}}, & \text{if } i + i' \neq 1 \text{ and } j + j' \neq 1 \\ \frac{(1 + s_{00,11})2x_{11,k}x_{00,k} + (1 + s_{01,10})2x_{10,k}x_{01,k}}{\sum_{i,j=0}^1 \sum_{i',j'=0}^1 (1 + s_{ij,i'j'})x_{i'j',k}x_{ij,k}}, & \text{if } i + i' = 1 \text{ and } j + j' = 1 \\ \frac{(1 + s_{ij,i'j'})2x_{i'j',k}x_{ij,k}}{\sum_{i,j=0}^1 \sum_{i',j'=0}^1 (1 + s_{ij,i'j'})x_{i'j',k}x_{ij,k}}, & \text{otherwise} \end{cases} \quad (13)$$

196 for $i, j, i', j' = 0, 1$.

197 The fourth term of the product in Eq. (10), $p(\mathbf{r}_{1:K} | \mathbf{g}_{1:K})$, is the probability of observing the
198 reads of all sampled individuals given their corresponding genotypes. Using the conditional in-
199 dependence from our HMM framework, as shown in Figure 1, we can decompose the probability
200 $p(\mathbf{r}_{1:K} | \mathbf{g}_{1:K})$ as

$$p(\mathbf{r}_{1:K} | \mathbf{g}_{1:K}) = \prod_{k=1}^K p(\mathbf{r}_k | \mathbf{g}_k) = \prod_{k=1}^K \prod_{n=1}^{N_k} p(\mathbf{r}_{n,k} | \mathbf{g}_{n,k}) = \prod_{k=1}^K \prod_{n=1}^{N_k} \prod_{l=1}^2 p(\mathbf{r}_{l,n,k} | g_{l,n,k}), \quad (14)$$

201 where $p(\mathbf{r}_{l,n,k} | g_{l,n,k})$ is the probability of observing the reads $\mathbf{r}_{l,n,k}$ of sampled individual n at
202 locus l given its genotype $g_{l,n,k}$, known as the genotype likelihood, which is commonly available
203 with aDNA data.

204 2.2.2. Adaptive particle marginal Metropolis-Hastings

205 Similar to He et al. (2022), we carry out our posterior computation by the PMMH algorithm
206 (Andrieu et al., 2010) that enables us to jointly update the selection coefficients and population
207 gamete frequency trajectories. More specifically, we estimate the marginal likelihood

$$p(\mathbf{r}_{1:K} | \boldsymbol{\vartheta}) = \int_{\Omega_{\mathbf{X}}^K} p(\mathbf{x}_{1:K} | \boldsymbol{\vartheta})p(\mathbf{g}_{1:K} | \mathbf{x}_{1:K})p(\mathbf{r}_{1:K} | \mathbf{g}_{1:K}) d\mathbf{x}_{1:K} \quad (15)$$

208 through the bootstrap particle filter (Gordon et al., 1993), where we generate the particles from
209 the Wright-Fisher SDE's in Eq. (8) by the Euler-Maruyama scheme. The product of the average
210 weights of the set of particles at the sampling time points $\mathbf{t}_{1:K}$ yields an unbiased estimate of
211 the marginal likelihood $p(\mathbf{r}_{1:K} | \boldsymbol{\vartheta})$, denoted by $\hat{p}(\mathbf{r}_{1:K} | \boldsymbol{\vartheta})$. The population gamete frequency
212 trajectories $\mathbf{x}_{1:K}$ are sampled once from the final set of particles with their relevant weights.

213 Although the PMMH algorithm has been shown to work well in He et al. (2022), in practice,

214 its performance depends strongly on the choice of the proposal. In this work, due to the increase
 215 in the number of selection coefficients required to be estimated, choosing an appropriate proposal
 216 to ensure computational efficiency becomes challenging. To resolve this issue, we adopt a random
 217 walk proposal with covariance matrix $\mathbf{\Gamma}$, denoted by $q(\cdot | \boldsymbol{\vartheta}; \mathbf{\Gamma})$, the Gaussian probability density
 218 function with mean vector $\boldsymbol{\vartheta}$ and covariance matrix $\mathbf{\Gamma}$, and under ideal conditions, the optimal
 219 choice of the covariance matrix $\mathbf{\Gamma}$ is a rescaled version of the covariance matrix of the posterior
 220 (Roberts & Rosenthal, 2001). Given that the covariance matrix of the posterior is commonly
 221 not available in advance, we adopt the adaptation strategy (Vihola, 2012) that can dynamically
 222 align the covariance matrix of the proposal with that of the posterior based on accepted samples.
 223 More specifically, we prespecify a target acceptance rate, denoted by A^* , and a step size sequence
 224 (decaying to zero), denoted $\{\eta^i\}_{i \geq 1}$, where the superscript denotes the iteration. The covariance
 225 matrix is updated by following the iteration formula

$$\mathbf{\Gamma}^i = \mathbf{\Gamma}^{i-1} + \eta^i (A^i - A^*) \frac{(\boldsymbol{\vartheta}^i - \boldsymbol{\vartheta}^{i-1})(\boldsymbol{\vartheta}^i - \boldsymbol{\vartheta}^{i-1})^\top}{\|\boldsymbol{\vartheta}^i - \boldsymbol{\vartheta}^{i-1}\|^2} \quad (16)$$

226 with the covariance matrix $\mathbf{\Gamma}^1$ (*e.g.*, $\mathbf{\Gamma}^1 = \sigma^2 \mathbf{I}$) and selection coefficients $\boldsymbol{\vartheta}^1 \sim p(\boldsymbol{\vartheta})$, where

$$\boldsymbol{\vartheta}^i \sim q(\boldsymbol{\vartheta} | \boldsymbol{\vartheta}^{i-1}; \mathbf{\Gamma}^{i-1}) \quad (17)$$

227 and

$$A^i = \frac{p(\boldsymbol{\vartheta}^i)}{p(\boldsymbol{\vartheta}^{i-1})} \frac{\hat{p}(\mathbf{r}_{1:K} | \boldsymbol{\vartheta}^i)}{\hat{p}(\mathbf{r}_{1:K} | \boldsymbol{\vartheta}^{i-1})} \frac{q(\boldsymbol{\vartheta}^{i-1} | \boldsymbol{\vartheta}^i; \mathbf{\Gamma}^{i-1})}{q(\boldsymbol{\vartheta}^i | \boldsymbol{\vartheta}^{i-1}; \mathbf{\Gamma}^{i-1})}. \quad (18)$$

228 Such an adaptation strategy can also coerce the acceptance rate. In practice, the target accep-
 229 tance rate is set to $A^* \in [0.234, 0.440]$, and the step size sequence is defined as $\eta^i = i^{-\gamma}$ with
 230 $\gamma \in (0.5, 1]$ (Vihola, 2012). See Luengo et al. (2020) and references therein for other adaptation
 231 strategies.

232 For the sake of clarity, we write down the robust adaptive version of the PMMH algorithm
 233 for our posterior computation:

234 Step 1: Initialise the selection coefficients $\boldsymbol{\vartheta}$ and population gamete frequency trajectories $\mathbf{x}_{1:K}$:

235 Step 1a: Draw $\boldsymbol{\vartheta}^1 \sim p(\boldsymbol{\vartheta})$.

236 Step 1b: Run a bootstrap particle filter with $\boldsymbol{\vartheta}^1$ to get $\hat{p}(\mathbf{r}_{1:K} | \boldsymbol{\vartheta}^1)$ and $\mathbf{x}_{1:K}^1$.

237 Step 1c: Initialise $\mathbf{\Gamma}^1$.

238 Repeat Step 2 until enough samples of the selection coefficients $\boldsymbol{\vartheta}$ and population gamete fre-
239 quency trajectories $\boldsymbol{x}_{1:K}$ have been attained:

240 Step 2: Update the selection coefficients $\boldsymbol{\vartheta}$ and population gamete frequency trajectories $\boldsymbol{x}_{1:K}$:

241 Step 2a: Draw $\boldsymbol{\vartheta}^i \sim q(\boldsymbol{\vartheta} \mid \boldsymbol{\vartheta}^{i-1}; \boldsymbol{\Gamma}^{i-1})$.

242 Step 2b: Run a bootstrap particle filter with $\boldsymbol{\vartheta}^i$ to get $\hat{p}(\boldsymbol{r}_{1:K} \mid \boldsymbol{\vartheta}^i)$ and $\boldsymbol{x}_{1:K}^i$.

243 Step 2c: Update $\boldsymbol{\Gamma}^i$ through Eqs. (16) and (18).

244 Step 2d: Accept $\boldsymbol{\vartheta}^i$ and $\boldsymbol{x}_{1:K}^i$ with A^i and set $\boldsymbol{\vartheta}^i = \boldsymbol{\vartheta}^{i-1}$ and $\boldsymbol{x}_{1:K}^i = \boldsymbol{x}_{1:K}^{i-1}$ otherwise.

245 With sufficiently large samples of the selection coefficients $\boldsymbol{\vartheta}$ and population gamete frequency
246 trajectories $\boldsymbol{x}_{1:K}$, we produce the minimum mean square error (MMSE) estimates for the selec-
247 tion coefficients $\boldsymbol{\vartheta}$ and population gamete frequency trajectories $\boldsymbol{x}_{1:K}$ through calculating their
248 posterior means.

249 As in He et al. (2022), our procedure can allow the selection coefficients $s_{ij,i'j'}$ to change over
250 time (piecewise constant), *e.g.*, let the selection coefficients $s_{ij,i'j'}(t) = s_{ij,i'j'}^-$ if $t < \tau$ otherwise
251 $s_{ij,i'j'}(t) = s_{ij,i'j'}^+$, where τ is the time of an event that might change selection, *e.g.*, the times of
252 plant and animal domestication. The only modification required is to simulate the population
253 gamete frequency trajectories $\boldsymbol{x}_{1:K}$ according to the Wright-Fisher diffusion with the selection
254 coefficients $s_{ij,i'j'}^-$ for $t < \tau$ and $s_{ij,i'j'}^+$ for $t \geq \tau$, respectively. In this setup, we propose a scheme
255 to test the hypothesis whether selection changes at time τ for each phenotypic trait, including
256 estimating their selection differences, through computing the posterior $p(\Delta s_{ij,i'j'} \mid \boldsymbol{r}_{1:K})$ from
257 the PMMH samples of the selection coefficients $s_{ij,i'j'}^-$ and $s_{ij,i'j'}^+$, where $\Delta s_{ij,i'j'} = s_{ij,i'j'}^+ - s_{ij,i'j'}^-$
258 denotes the change in the selection coefficient at time τ . Note that our method enables us to deal
259 with the case that the events that might change selection are different for different phenotypic
260 traits (*i.e.*, the time τ could be taken to be different values for different phenotypic traits).

261 3. Results

262 In this section, we employ our approach to reanalyse the published ancient horse DNA data
263 from earlier studies of Ludwig et al. (2009), Pruvost et al. (2011) and Wutke et al. (2016), where
264 they sequenced 201 ancient horse samples in total ranging from a pre- to a post-domestication
265 period for eight loci coding for horse coat colouration. In particular, we perform the inference of

266 selection acting on the base coat colour controlled by *ASIP* and *MC1R* and the pinto coat pat-
267 tern determined by *KIT13* and *KIT16*. Extensive simulation studies, supporting the accuracy
268 of our methodology, are available in the supplement.

269 As Wutke et al. (2016) only provided called genotypes for each gene (including missing calls),
270 we use the same scheme as in He et al. (2022) to convert to corresponding genotype likelihoods.
271 More specifically, we take the genotype likelihood of the called genotype to be 1 and those of the
272 remaining two to be 0 if the genotype is called, and otherwise, all possible (ordered) genotypes
273 are assigned equal genotype likelihoods (normalised to sum to 1). Genotype likelihoods for each
274 gene can be found in Supplementary Information, Table S1.

275 In what follows, we take the average length of a generation of the horse to be eight years and
276 use the time-varying size of the horse population estimated by Der Sarkissian et al. (2015) (see
277 Supplementary Information, Figure S1) with the reference population size $N_0 = 16000$ (*i.e.*, the
278 most recent population size) like Schraiber et al. (2016) unless otherwise noted. Given that the
279 flat Dirichlet prior for the starting frequencies of the gametes in the underlying population is
280 more likely to produce low linkage disequilibrium, we generate the starting population gamete
281 frequencies \mathbf{x}_1 through the following procedure:

282 Step 1: Draw $y_1, y_2 \sim \text{Uniform}(0, 1)$.

283 Step 2: Draw $D \sim \text{Uniform}(\max\{-y_1y_2, -(1 - y_1)(1 - y_2)\}, \min\{y_1(1 - y_2), (1 - y_1)y_2\})$.

284 Step 3: Set $\mathbf{x}_1 = ((1 - y_1)(1 - y_2) + D, (1 - y_1)y_2 - D, y_1(1 - y_2) - D, y_1y_2 + D)$.

285 Note that y_1 and y_2 denote the starting population frequencies of the mutant allele at the two
286 loci, respectively, and D is the coefficient of linkage disequilibrium. We run our adaptive PMMH
287 algorithm with 1000 particles and 20000 iterations, where we set the target acceptance rate to
288 $A^* = 0.4$ and define the step size sequence as $\eta_i = i^{-2/3}$ for $i = 1, 2, \dots, 20000$. We divide each
289 generation into five subintervals in the Euler-Maruyama scheme. We discard a burn-in of 10000
290 iterations and thin the remaining iterations by keeping every fifth value.

291 3.1. Horse base coat colours

292 The horse genes *ASIP* and *MC1R* are primarily responsible for determination of base coat
293 colours (*i.e.*, bay, black and chestnut). The *ASIP* gene is located on chromosome 22, whereas
294 the *MC1R* gene is located on chromosome 3. At each locus, there are two allele types, labelled

295 A and a for $ASIP$ and E and e for $MC1R$, respectively, where the capital letter represents the
 296 ancestral allele and the small letter represents the mutant allele. See Table 1 for the genotype-
 297 phenotype map at $ASIP$ and $MC1R$ for horse base coat colours. Notice that $MC1R$ is epistatic
 298 to $ASIP$ (Rieder et al., 2001).

		$MC1R$		
		E/E	E/e	e/e
$ASIP$	A/A	bay	bay	chestnut
	A/a	bay	bay	chestnut
	a/a	black	black	chestnut

Table 1: The genotype-phenotype map at $ASIP$ and $MC1R$ for horse base coat colours.

299 3.1.1. Wright-Fisher diffusion for $ASIP$ and $MC1R$

300 Let us consider a horse population represented by the alleles at $ASIP$ and $MC1R$ evolving
 301 under selection over time, which induces four possible haplotypes AE , Ae , aE and ae , labelled
 302 haplotypes 00, 01, 01 and 11, respectively. We take the relative viabilities of the three pheno-
 303 types, *i.e.*, the bay, black and chestnut coat, to be 1, $1 + s_b$ and $1 + s_c$, respectively, where s_b is
 304 the selection coefficient of the black coat against the bay coat and s_c is the selection coefficient
 305 of the chestnut coat against the bay coat. See Table 2 for the relative viabilities of all genotypes
 306 at $ASIP$ and $MC1R$.

	AE	Ae	aE	ae
AE	1	1	1	1
Ae	1	$1 + s_c$	1	$1 + s_c$
aE	1	1	$1 + s_b$	$1 + s_b$
ae	1	$1 + s_c$	$1 + s_b$	$1 + s_c$

Table 2: Relative viabilities of all genotypes at $ASIP$ and $MC1R$.

307 We measure time in units of $2N_0$ generations and scale the selection coefficients $\alpha_b = 2N_0s_b$,
 308 $\alpha_c = 2N_0s_c$ and recombination rate $\rho = 4N_0r$, respectively. Let $X_{ij}(t)$ be the gamete frequency
 309 of haplotype ij at time t , which satisfies the Wright-Fisher SDE's in Eq. (8). More specifically,

310 the drift term $\boldsymbol{\mu}(t, \boldsymbol{x})$ can be simplified with the genotype-phenotype map shown in Table 2 as

$$\begin{aligned}\mu_{00}(t, \boldsymbol{x}) &= -\alpha_b x_{10}(x_{00}x_{11} + x_{00}x_{1*}) - \alpha_c x_{00}x_{*1}x_{*1} - \frac{\rho}{2}(x_{00}x_{11} - x_{01}x_{10}) \\ \mu_{01}(t, \boldsymbol{x}) &= -\alpha_b x_{10}(x_{01}x_{11} + x_{01}x_{1*}) + \alpha_c x_{01}x_{*0}x_{*1} + \frac{\rho}{2}(x_{00}x_{11} - x_{01}x_{10}) \\ \mu_{10}(t, \boldsymbol{x}) &= -\alpha_b x_{10}(x_{10}x_{11} + x_{10}x_{1*} - x_{1*}) - \alpha_c x_{10}x_{*1}x_{*1} + \frac{\rho}{2}(x_{00}x_{11} - x_{01}x_{10}) \\ \mu_{11}(t, \boldsymbol{x}) &= -\alpha_b x_{10}(x_{11}x_{11} + x_{11}x_{1*} - x_{11}) + \alpha_c x_{11}x_{*0}x_{*1} - \frac{\rho}{2}(x_{00}x_{11} - x_{01}x_{10}),\end{aligned}\tag{19}$$

311 where we take the scaled recombination rate to be $\rho = 2N_0$ since the two genes are located on
312 separate chromosomes.

313 3.1.2. Selection of horse base coat colours

314 We use our method to test the null hypothesis that no change occurred in selection acting on
315 base coat colours when horses became domesticated (in approximately 3500 BC) and estimate
316 their selection intensities and changes. We restrict our study to the period from the start of the
317 Holocene epoch (around 9700 BC) onwards and assume that the respective mutations occurred
318 at both *ASIP* and *MC1R* before 9700 BC. Given that *ASIP* and *MC1R* are located on separate
319 chromosomes, we generate the initial population gamete frequencies by following the procedure
320 described above but fix the coefficient of linkage disequilibrium to zero. The resulting posteriors
321 for the selection coefficients and underlying phenotype frequency trajectories of the population
322 are shown in Figure 2, and their estimates as well as the 95% highest posterior density (HPD)
323 intervals are summarised in Supplementary Information, Table S2.

324 Our estimate for the selection coefficient of the black coat is 0.0003 with 95% HPD interval
325 $[-0.0047, 0.0053]$ from the beginning of the Holocene epoch and 0.0003 with 95% HPD interval
326 $[-0.0028, 0.0036]$ after horses became domesticated. Our estimate for the change in the selection
327 coefficient is around 0 with 95% HPD interval $[-0.0072, 0.0060]$. The posteriors for the selection
328 coefficients s_b^- and s_b^+ and their difference Δs_b are all approximately symmetric about 0, which
329 implies that the black coat was selectively neutral over the Holocene epoch, and no change took
330 place in selection of the black coat from a pre- to a post-domestication period. Our estimate for
331 the underlying frequency trajectory of the black coat illustrates that it keeps roughly constant
332 through time, although with a slight decrease after horses were domesticated.

333 In the pre-domestication period, our estimate for the selection coefficient of the chestnut coat

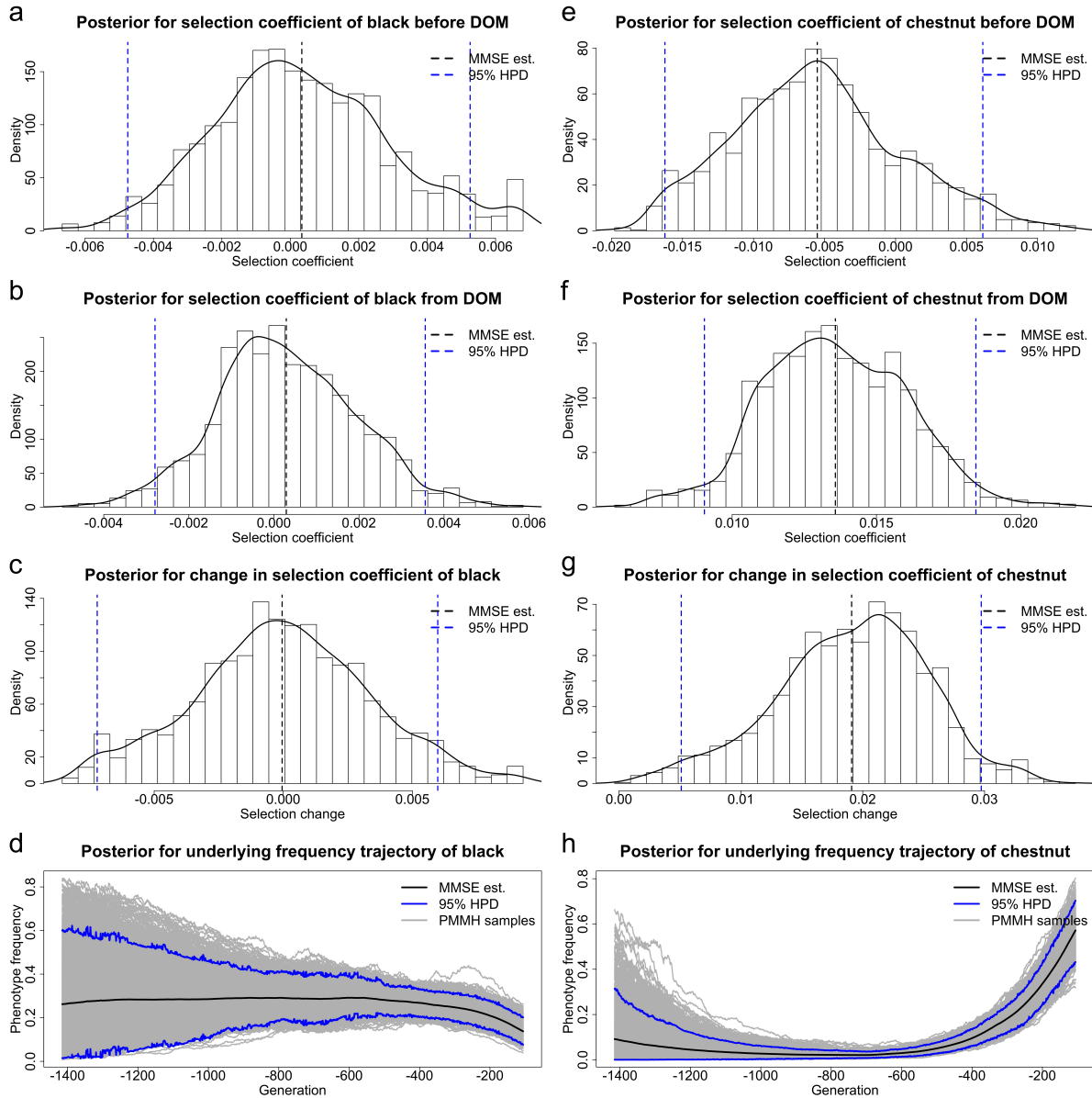


Figure 2: Posteriors for selection of horse base coat colours before and from horse domestication (starting from 3500 BC) and underlying frequency trajectories of each phenotypic trait in the population, (a)-(d) for the black coat and (e)-(h) for the chestnut coat, respectively. The samples drawn before 9700 BC, the starting time of the Holocene, are excluded. DOM stands for domestication.

334 is -0.0055 with 95% HPD interval $[-0.0162, 0.0061]$. Although the 95% HPD interval contains
 335 0, we still find that the chestnut coat was most probably selectively deleterious (with posterior
 336 probability for negative selection being 0.818). In the post-domestication period, our estimate
 337 for the selection coefficient of the chestnut coat is 0.0136 with 95% HPD interval $[0.0090, 0.0184]$,
 338 suggesting that the chestnut coat was positively selected (with posterior probability for positive
 339 selection being 1.000). Combining our estimate for the change in the selection coefficient being
 340 0.0191 with 95% HPD interval $[0.0051, 0.0297]$, we observe sufficient evidence to support that a

341 positive change took place in selection of the chestnut coat when horses were domesticated. Our
 342 estimate for the underlying frequency trajectory of the chestnut coat reveals a slow fall from the
 343 beginning of the Holocene epoch and then a significant rise after horses became domesticated.

344 We also provide the results produced with a flat Dirichlet prior for the starting population
 345 gamete frequencies (see Supplementary Information, Figure S2 and Table S3). The results for
 346 selection acting on the black and chestnut coats are consistent with those shown in Figure 2.

347 3.2. Horse pinto coat patterns

348 The horse genes *KIT13* and *KIT16* are mainly responsible for determination of pinto coat
 349 patterns (*i.e.*, tobiano and sabino), both of which reside on chromosome 3, 4668 base pairs (bp)
 350 apart, with the average rate of recombination 10^{-8} crossover/bp (Dumont & Payseur, 2008).
 351 At each locus, there are two allele types, labelled *KM0* for the ancestral allele and *KM1* for the
 352 mutant allele at *KIT13* and *sb1* for the ancestral allele and *SB1* for the mutant allele at *KIT16*,
 353 respectively. See Table 3 for the genotype-phenotype map at *KIT13* and *KIT16* for horse pinto
 354 coat patterns. Note that the coat pattern, called solid, refers to a coat that neither tobiano nor
 355 sabino is present, and the coat pattern, called mixed, refers to a coat that is a mixture between
 356 tobiano and sabino.

		<i>KIT16</i>		
		<i>sb1/sb1</i>	<i>sb1/SB1</i>	<i>SB1/SB1</i>
<i>KIT13</i>	<i>KM0/KM0</i>	solid	sabino	sabino
	<i>KM0/KM1</i>	tobiano	mixed	mixed
	<i>KM1/KM1</i>	tobiano	mixed	mixed

Table 3: The genotype-phenotype map at *KIT13* and *KIT16* for horse pinto coat patterns.

357 3.2.1. Wright-Fisher diffusion for *KIT13* and *KIT16*

358 We now consider a horse population represented by the alleles at *KIT13* and *KIT16* evolving
 359 under selection over time. Such a setup gives rise to four possible haplotypes *KM0sb1*, *KM0SB1*,
 360 *KM1sb1* and *KM1SB1*, labelled haplotypes 00, 01, 01 and 11, respectively. We take the relative
 361 viabilities of the four phenotypes, *i.e.*, the solid, tobiano, sabino and mixed coat, to be 1, $1 + s_{to}$,
 362 $1 + s_{sb}$ and $1 + s_{mx}$, respectively, where s_{to} is the selection coefficient of the tobiano coat against
 363 the solid coat, s_{sb} is the selection coefficient of the sabino coat against the solid coat, and s_{mx}

364 is the selection coefficient of the mixed coat against the solid coat. See Table 4 for the relative
 365 viabilities of all genotypes at *KIT13* and *KIT16*.

	<i>KM0sb1</i>	<i>KM0SB1</i>	<i>KM1sb1</i>	<i>KM1SB1</i>
<i>KM0sb1</i>	1	$1 + s_{sb}$	$1 + s_{to}$	$1 + s_{mx}$
<i>KM0SB1</i>	$1 + s_{sb}$	$1 + s_{sb}$	$1 + s_{mx}$	$1 + s_{mx}$
<i>KM1sb1</i>	$1 + s_{to}$	$1 + s_{mx}$	$1 + s_{to}$	$1 + s_{mx}$
<i>KM1SB1</i>	$1 + s_{mx}$	$1 + s_{mx}$	$1 + s_{mx}$	$1 + s_{mx}$

Table 4: Relative viabilities of all genotypes at *KIT13* and *KIT16*.

366 We measure time in units of $2N_0$ generations and scale the selection coefficients $\alpha_{to} = 2N_0s_{to}$,
 367 $\alpha_{sb} = 2N_0s_{sb}$, $\alpha_{mx} = 2N_0s_{mx}$ and recombination rate $\rho = 4N_0r$, respectively. Let $X_{ij}(t)$ be the
 368 gamete frequency of haplotype ij at time t , which follows the Wright-Fisher SDE's in Eq. (8).
 369 In particular, the drift term $\boldsymbol{\mu}(t, \mathbf{x})$ can be simplified with the genotype-phenotype map shown
 370 in Table 4 as

$$\begin{aligned}
 \mu_{00}(t, \mathbf{x}) &= -\alpha_{to}x_{00}(x_{10}(x_{00} + x_{*0}) - x_{10}) - \alpha_{sb}x_{00}(x_{01}(x_{00} + x_{0*}) - x_{01}) \\
 &\quad - \alpha_{mx}x_{00}(2x_{01}x_{10} + x_{11} - x_{11}^2) - \frac{\rho}{2}(x_{00}x_{11} - x_{01}x_{10}) \\
 \mu_{01}(t, \mathbf{x}) &= -\alpha_{to}x_{01}x_{10}(x_{00} + x_{*0}) - \alpha_{sb}x_{01}(x_{01}(x_{00} + x_{0*}) - x_{0*}) \\
 &\quad - \alpha_{mx}x_{01}((2x_{01}x_{10} + x_{11} - x_{11}^2) - x_{10}) + \frac{\rho}{2}(x_{00}x_{11} - x_{01}x_{10}) \\
 \mu_{10}(t, \mathbf{x}) &= -\alpha_{to}x_{10}(x_{10}(x_{00} + x_{*0}) - x_{*0}) - \alpha_{sb}x_{10}x_{01}(x_{00} + x_{0*}) \\
 &\quad - \alpha_{mx}x_{10}((2x_{01}x_{10} + x_{11} - x_{11}^2) - x_{01}) + \frac{\rho}{2}(x_{00}x_{11} - x_{01}x_{10}) \\
 \mu_{11}(t, \mathbf{x}) &= -\alpha_{to}x_{11}x_{10}(x_{00} + x_{*0}) - \alpha_{sb}x_{11}x_{01}(x_{00} + x_{0*}) \\
 &\quad - \alpha_{mx}x_{11}((2x_{01}x_{10} + x_{11} - x_{11}^2) - (1 - x_{11})) - \frac{\rho}{2}(x_{00}x_{11} - x_{01}x_{10}).
 \end{aligned} \tag{20}$$

371 3.2.2. Selection of horse pinto coat patterns

372 We apply our method to test the null hypothesis that no change took place in selection acting
 373 on horse pinto coat patterns when the medieval period began (in around AD 400) and estimate
 374 their selection intensities and changes. We restrict our study to the period from the beginning
 375 of horse domestication (around 3500 BC) onwards and assume that the respective mutations
 376 occurred at both *KIT13* and *KIT16* before 3500 BC. To our knowledge, the mixed coat has never
 377 been found in the horse population, and we therefore fix the selection coefficient $s_{mx} = -1$ over
 378 time. The resulting posteriors for the selection coefficients and underlying phenotype frequency

379 trajectories of the population are illustrated in Figure 3, and their estimates as well as the 95%
 380 HPD intervals are summarised in Supplementary Information, Table S4.

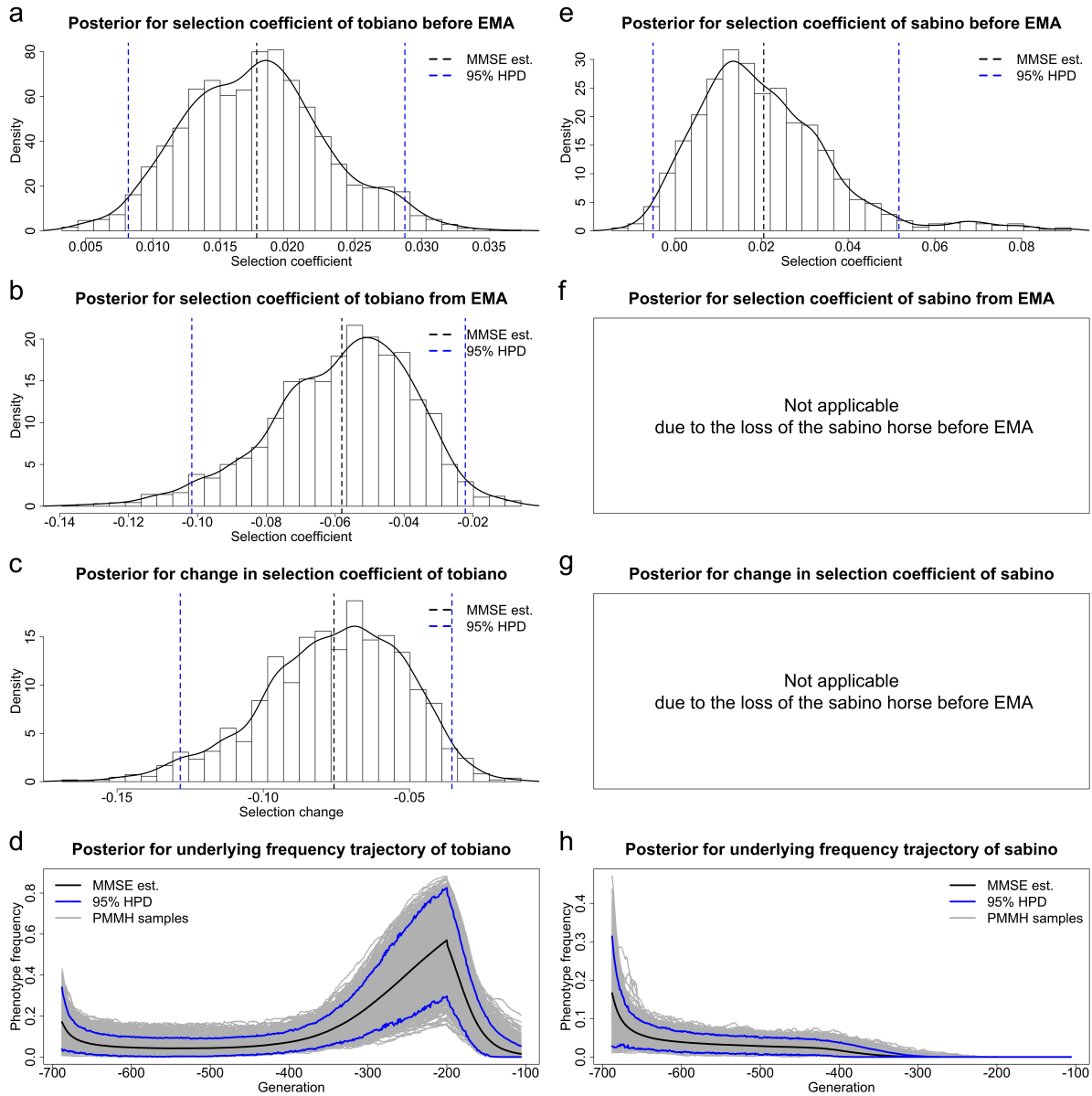


Figure 3: Posteriors for selection of horse pinto coat patterns before and from the medieval period (starting from AD 400) and underlying frequency trajectories of each phenotypic trait in the population, (a)-(d) for the tobiano coat and (e)-(h) for the sabino coat, respectively. The samples drawn before 3500 BC, the starting time of horse domestication, are excluded. EMA stands for Early Middle Ages.

381 Our estimate for the selection coefficient of the tobiano coat is 0.0177 with 95% HPD interval
 382 [0.0082, 0.0287] from the beginning of horse domestication and -0.0581 with 95% HPD interval
 383 $[-0.1016, -0.0222]$ in the Middle Ages. Our estimates reveal sufficient evidence to support that
 384 the tobiano coat was positively selected after horses were domesticated but became negatively
 385 selected in the Middle Ages. Our estimate for the change in the selection coefficient is -0.0758

386 with 95% HPD interval $[-0.1284, -0.0355]$, which illustrates that a negative change took place
387 in selection of the tobiano coat when the Middle Ages started. Our estimate for the underlying
388 frequency trajectory of the tobiano coat indicates that the frequency of the tobiano coat grows
389 substantially after horses were domesticated and then drops sharply during the medieval period.

390 Our estimate for the selection coefficient of the sabino coat is 0.0206 with 95% HPD interval
391 $[-0.0050, 0.0517]$ before the Middle Ages, which shows compelling evidence of positive selection
392 acting on the sabino coat (with posterior probability for positive selection being 0.945). However,
393 we see that the frequency of the sabino coat declines slowly from the start of horse domestication
394 until the loss of the sabino coat in approximately 120 BC (*i.e.*, the earliest time that the upper
395 and lower bounds of the 95% HPD interval for the frequency of the sabino coat are both zero),
396 probably resulting from that the sabino coat was somewhat out-competed by the tobiano coat
397 under the tight linkage between *KIT13* and *KIT16*.

398 Note, here we only present the resulting posterior for the selection coefficient s_{sb}^- . This is
399 because our results show that the sabino coat became extinct before the medieval period (see
400 Figure 3h). Without genetic variation data, the PMMH algorithm fails to converge in reasonable
401 time for the selection coefficient s_{sb}^+ , which however does not affect estimation of the remaining
402 three selection coefficients (see Supplementary Information, Figure S3, where we repeatedly run
403 our procedure to estimate the selection coefficients s_{to}^- , s_{to}^+ and s_{sb}^- with different prespecified
404 values of the selection coefficient s_{sb}^+ that are uniformly drawn from $[-1, 1]$).

405 We also provide the results produced with a flat Dirichlet prior for the starting population
406 gamete frequencies (see Supplementary Information, Figure S4 and Table S5) and the results
407 that we co-estimate the selection coefficient of the mixed coat (see Supplementary Information,
408 Figure S5 and Table S6). Our estimate for the selection coefficient of the mixed coat is -0.5621
409 with 95% HPD interval $[-0.9645, -0.2262]$ before the Middle Ages. Such strong negative selec-
410 tion resulted in a quick loss of the mixed coat right after the domestication of the horse, which
411 we can also find from our estimate for the underlying frequency trajectory of the mixed coat.
412 The results for selection acting on the tobiano and sabino coats are consistent with those shown
413 in Figure 3.

414 4. Discussion

415 To overcome a fundamental limitation of He et al. (2022), which did not aim to model genetic
416 interactions, we presented a novel Bayesian approach for inferring temporally variable selection
417 from the data on aDNA sequences with the flexibility of modelling linkage and epistasis in this
418 work. Our method was mainly built upon the two-layer HMM framework of He et al. (2022), but
419 we introduced a Wright-Fisher diffusion to describe the underlying evolutionary dynamics of two
420 linked genes subject to phenotypic selection, which was modelled through the differential fitness
421 of different phenotypic traits with a genotype-phenotype map. Such an HMM framework allows
422 us to account for two-gene interactions and sample uncertainties resulting from the damage and
423 fragmentation of aDNA molecules. Our posterior computation was carried out through a robust
424 adaptive PMMH algorithm to guarantee computational efficiency. Unlike the original version of
425 the PMMH of Andrieu et al. (2010), the adaption rule of Vihola (2012) was introduced to tune
426 the covariance structure of the proposal to obtain a coerced acceptance rate in our procedure.
427 Moreover, our method permits the reconstruction of the underlying population gamete frequency
428 trajectories and offers the flexibility of modelling time-varying demographic histories.

429 We reanalysed the horse coat colour genes, *e.g.*, the *ASIP* and *MC1R* genes associated with
430 base coat colours and the *KIT13* and *KIT16* genes associated with pinto coat patterns, based
431 on the ancient horse samples from previous studies of Ludwig et al. (2009), Pruvost et al. (2011)
432 and Wutke et al. (2016). Our findings match the previous studies that the coat colour change in
433 the horse is considered as a domestic trait that was subject to early selection by humans (Hunter,
434 2018), *e.g.*, *ASIP* and *MC1R*, and human preferences have significantly changed over time and
435 across cultures (Wutke et al., 2016), *e.g.*, *KIT13* and *KIT16*. Our results were validated through
436 extensive simulations that mimicked the ancient horse samples (see Supplementary Information,
437 File S2, where we also provide simulation studies on performance evaluation).

438 For base coat colours, we conclude that there is not enough evidence available to reject the
439 null hypotheses that the black coat was selectively neutral from a pre- to a post-domestication
440 period and no change occurred in selection of the black coat when horses became domesticated.
441 However, our results provide sufficient evidence to support that the chestnut coat was effectively
442 neutral or experienced weak negative selection until the beginning of horse domestication and
443 then became favoured by selection. We see strong evidence of such a positive change in selection

444 of the chestnut coat occurring when horse domestication started, which matches the findings in
445 previous studies that selection for noncamouflaged coats might not have taken place until after
446 horses were domesticated (see Larson & Fuller, 2014, and references therein).

447 For pinto coat patterns, we show strong evidence of positive selection acting on the tobiano
448 and sabino coats before the Middle Ages. However, the frequency of the sabino coat continuously
449 decreased from domestication until none was left (before the Middle Ages), probably because the
450 sabino coat was somewhat out-competed by the tobiano coat under tight linkage. The tobiano
451 coat became negatively selected during the Middle Ages. Our findings match the archaeological
452 evidence and historical records that spotted horses experienced early selection by humans but
453 the preference changed during the Middle Ages (see Wutke et al., 2016, and references therein).

454 To demonstrate the improvement attainable through modelling genetic interactions, we show
455 the resulting posteriors for the *ASIP* and *MC1R* genes in Figure 4 and the *KIT13* and *KIT16*
456 genes in Figure 5, respectively, which are produced through the approach of He et al. (2022)
457 with the same settings as used in our adaptive PMMH algorithm. We summarise the results for
458 horse base coat colours and pinto coat patterns with their 95% HPD intervals in Supplementary
459 Information, Tables S7 and S8, respectively. Moreover, additional simulation studies are left in
460 Supplementary Information, File S3 to further show the improvement resulting from modelling
461 linkage and epistasis.

462 For base coat colours, we see from Figure 4 that the resulting posteriors for *ASIP* are similar
463 to those shown in Figure 2, which indicate that black horses were selectively neutral over the
464 Holocene epoch and no change occurred in selection of the black coat when horse domestication
465 started. However, since the method of He et al. (2022) ignores epistatic interaction, some geno-
466 types are incorrectly attributed to the black coat, which could alter the result of the inference
467 of selection. As illustrated in Figure 4, the resulting posteriors for *MC1R* suggest that chestnut
468 horses experienced positive selection from the start of the Holocene epoch onwards (with poste-
469 rior probabilities for positive selection being 0.636 in the pre-domestication period and 1.000 in
470 the post-domestication period, respectively). The evidence of a positive change that took place
471 in selection of the chestnut coat when horses were domesticated is no longer sufficient (*i.e.*, the
472 posterior probability is 0.430 for a positive change).

473 For pinto coat patterns, as illustrated in Figure 5, we see that tobiano horses were favoured

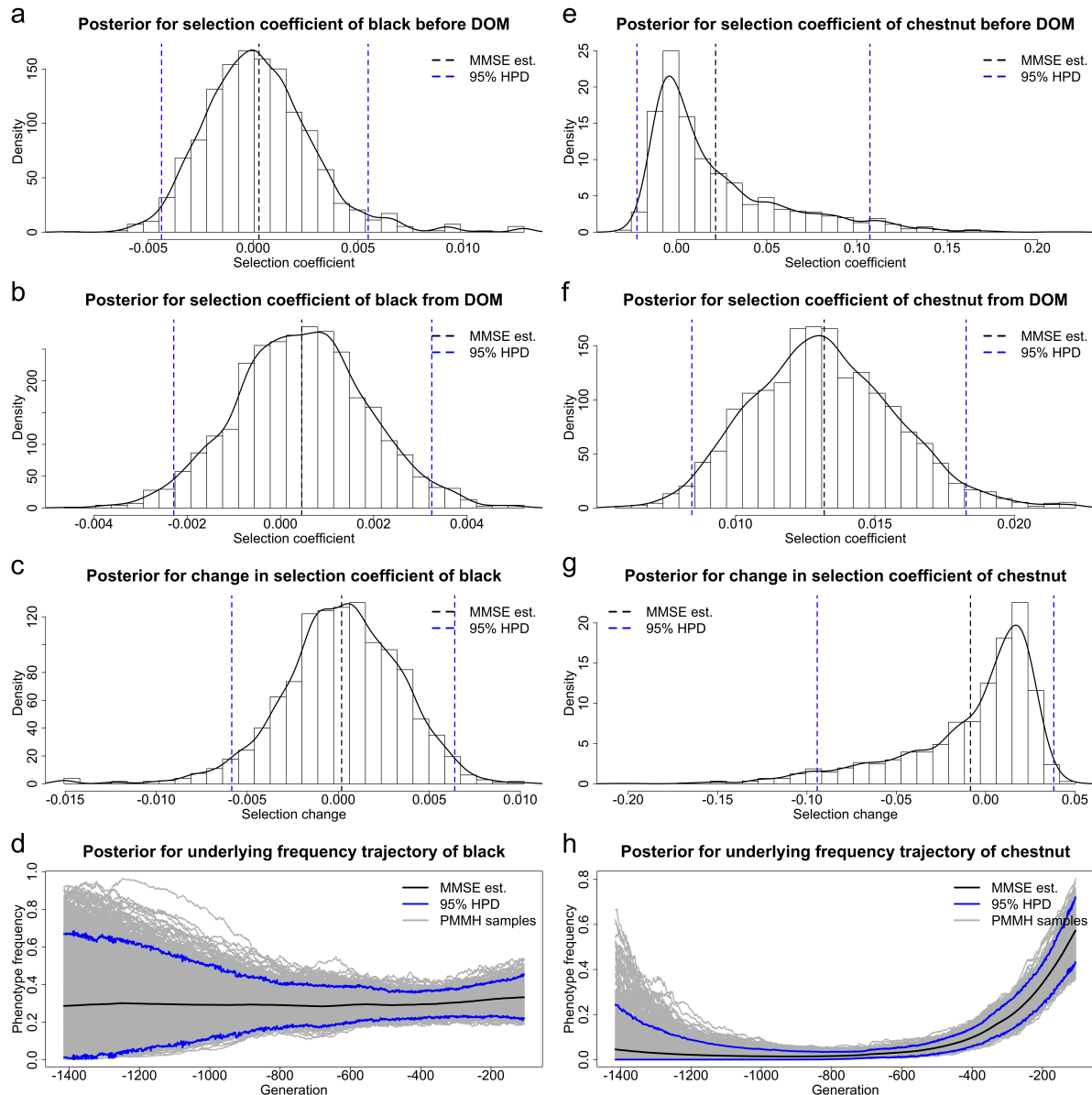


Figure 4: Posteriors for selection of horse base coat colours before and from horse domestication (starting from 3500 BC) and underlying frequency trajectories of each phenotypic trait in the population produced through the method of He et al. (2022), (a)-(d) for the black coat and (e)-(h) for the chestnut coat, respectively. The samples drawn before 9700 BC, the starting time of the Holocene, are excluded. DOM stands for domestication.

474 by selection since horse domestication started (with posterior probability for positive selection
 475 being 0.969) but became negatively selected during the Middle Ages (with posterior probability
 476 for negative selection being 0.983). We also find sufficient evidence against the null hypothesis
 477 that no change took place in selection of the tobiano coat when the medieval period started (with
 478 posterior probability for a negative change being 0.987). Our results for *KIT13* are compatible
 479 with those shown in Figure 3, but our results for *KIT16* are not. We observe from Figure 5 that
 480 sabino horses experienced negative selection from domestication until extinction that occurred

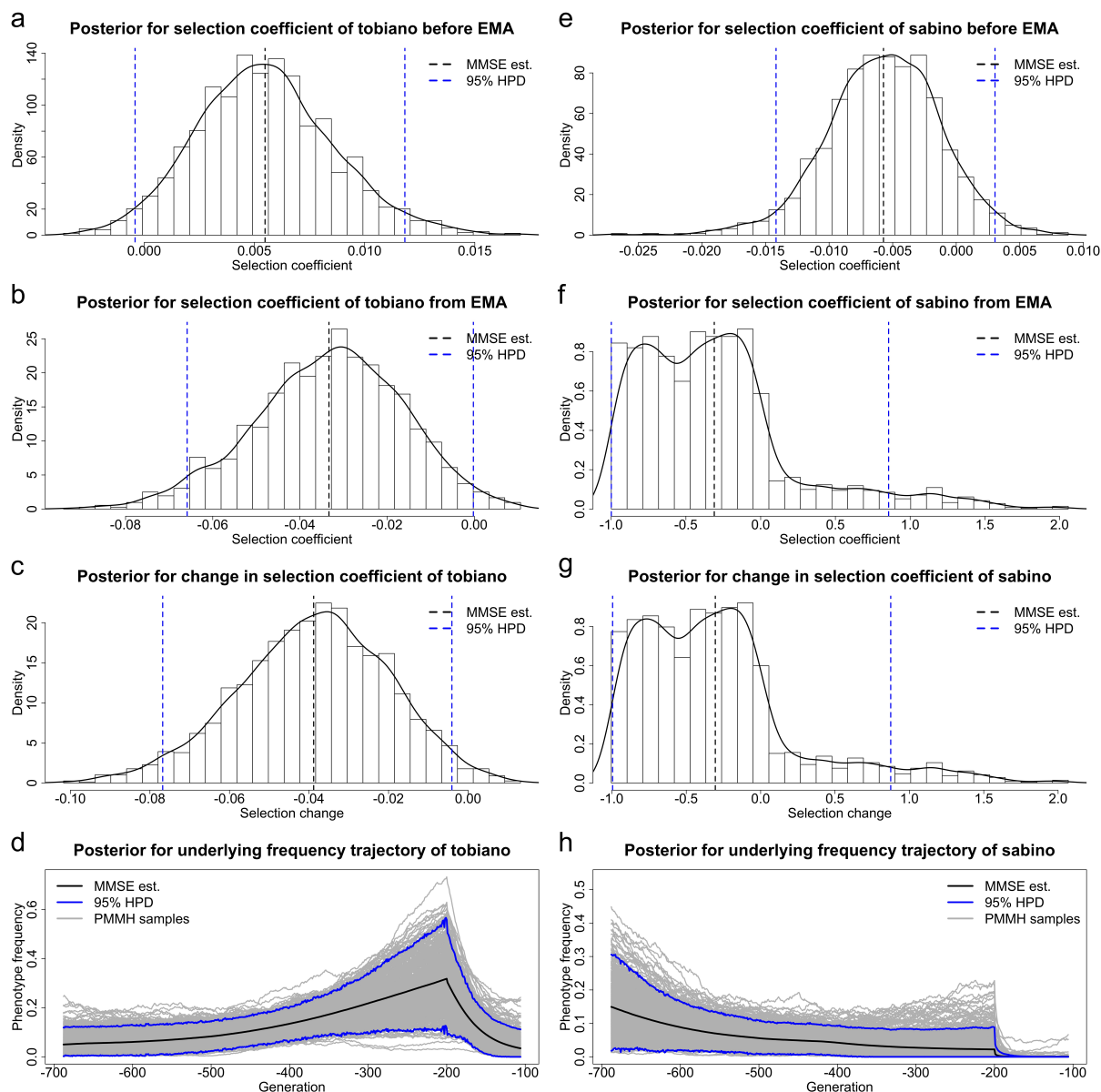


Figure 5: Posteriors for selection of horse pinto coat patterns before and from the medieval period (starting from AD 400) and underlying frequency trajectories of each phenotypic trait in the population produced through the method of He et al. (2022), (a)-(d) for the tobiano coat and (e)-(h) for the sabino coat, respectively. The samples drawn before 3500 BC, the starting time of horse domestication, are excluded. EMA stands for Early Middle Ages.

481 during the Middle Ages (see Figure 5h), which means that a continuous decline in sabino horses
 482 from domestication onwards was as a result of negative selection. However when we take genetic
 483 linkage into account, we find from Figure 3 that sabino horses were favoured by selection before
 484 the Middle Ages, and such a decline was probably triggered by the sabino coat being somewhat
 485 out-competed by the tobiano coat.

486 Our extension inherits desirable features of He et al. (2022) along with their key limitation

487 that all samples were assumed to be drawn after the mutant allele was created at both loci. Since
488 allele age is usually unavailable, we have to restrict our inference to a certain time window, *e.g.*,
489 from the time after which the mutant alleles at both loci have been observed in the sample or
490 the time before which we assume that the mutant alleles at both loci have already existed in the
491 population, which could largely alter the result of the inference of selection. As discussed in He
492 et al. (2020b) and He et al. (2022), one possible way of addressing this issue is to jointly estimate
493 the allele age like Malaspinas et al. (2012), Schraiber et al. (2016) and He et al. (2020c), which
494 however becomes cumbersome as there are many scenarios to consider in modelling and suffers
495 from particle degeneracy and sample impoverishment problems in the PMMH-based procedure.
496 An important consideration is that backward-in-time simulation of the Wright-Fisher diffusion
497 (Griffiths, 2003; Coop & Griffiths, 2004) is expected to address this challenge. In addition, how
498 to extend our work to handle the case of multiple interacting genes (Terhorst et al., 2015) and
499 estimate selection coefficients and their timing of changes (Shim et al., 2016; Mathieson, 2020)
500 will also be the topic of future investigation.

501 **Acknowledgements**

502 This work was carried out using the computational facilities of the Advanced Computing
503 Research Centre, University of Bristol - <http://www.bristol.ac.uk/acrc/>.

504 **References**

- 505 Allentoft, M. E., Sikora, M., Sjogren, K.-G., Rasmussen, S., Rasmussen, M. et al. (2015).
506 Population genomics of Bronze Age Eurasia. *Nature*, *522*, 167–172.
- 507 Alves, J. M., Carneiro, M., Cheng, J. Y., de Matos, A. L., Rahman, M. M. et al. (2019). Parallel
508 adaptation of rabbit populations to myxoma virus. *Science*, *363*, 1319–1326.
- 509 Andrieu, C., Doucet, A., & Holenstein, R. (2010). Particle Markov chain Monte Carlo methods.
510 *Journal of the Royal Statistical Society: Series B (Statistical Methodology)*, *72*, 269–342.
- 511 Bank, C., Ewing, G. B., Ferrer-Admettla, A., Foll, M., & Jensen, J. D. (2014). Thinking too
512 positive? Revisiting current methods of population genetic selection inference. *Trends in*
513 *Genetics*, *30*, 540–546.

- 514 Bollback, J. P., York, T. L., & Nielsen, R. (2008). Estimation of $2N_e s$ from temporal allele
515 frequency data. *Genetics*, *179*, 497–502.
- 516 Coop, G., & Griffiths, R. C. (2004). Ancestral inference on gene trees under selection. *Theoretical*
517 *Population Biology*, *66*, 219–232.
- 518 Corbin, L. J., Pope, J., Sanson, J., Antczak, D. F., Miller, D. et al. (2020). An independent
519 locus upstream of *ASIP* controls variation in the shade of the bay coat colour in horses.
520 *Genes*, *11*, 606.
- 521 Darwin, C. (1859). *On the Origin of Species by Means of Natural Selection, or the Preservation*
522 *of Favoured Races in the Struggle for Life*. London: John Murray.
- 523 Dehasque, M., Ávila-Arcos, M. C., Díez-del Molino, D., Fumagalli, M., Guschanski, K. et al.
524 (2020). Inference of natural selection from ancient DNA. *Evolution Letters*, *4*, 94–108.
- 525 Der Sarkissian, C., Ermini, L., Schubert, M., Yang, M. A., Librado, P. et al. (2015). Evolutionary
526 genomics and conservation of the endangered Przewalski’s horse. *Current Biology*, *25*, 2577–
527 2583.
- 528 Dumont, B. L., & Payseur, B. A. (2008). Evolution of the genomic rate of recombination in
529 mammals. *Evolution*, *62*, 276–294.
- 530 Fages, A., Hanghøj, K., Khan, N., Gaunitz, C., Seguin-Orlando, A. et al. (2019). Tracking
531 five millennia of horse management with extensive ancient genome time series. *Cell*, *177*,
532 1419–1435.
- 533 Ferrer-Admetlla, A., Leuenberger, C., Jensen, J. D., & Wegmann, D. (2016). An approximate
534 Markov model for the Wright-Fisher diffusion and its application to time series data. *Genetics*,
535 *203*, 831–846.
- 536 Fisher, R. A. (1922). On the dominance ratio. *Proceedings of the Royal Society of Edinburgh*,
537 *42*, 321–341.
- 538 Gordon, N. J., Salmond, D. J., & Smith, A. F. M. (1993). Novel approach to nonlinear/non-
539 Gaussian Bayesian state estimation. *IEE Proceedings F (Radar and Signal Processing)*, *140*,
540 107–113.

- 541 Griffiths, R. C. (2003). The frequency spectrum of a mutation, and its age, in a general diffusion
542 model. *Theoretical Population Biology*, *64*, 241–251.
- 543 He, Z., Beaumont, M. A., & Yu, F. (2017). Effects of the ordering of natural selection and
544 population regulation mechanisms on Wright-Fisher models. *G3: Genes, Genomes, Genetics*,
545 *7*, 2095–2106.
- 546 He, Z., Beaumont, M. A., & Yu, F. (2020a). Numerical simulation of the two-locus Wright-Fisher
547 stochastic differential equation with application to approximating transition probability den-
548 sities. *bioRxiv*, (p. 213769).
- 549 He, Z., Dai, X., Beaumont, M. A., & Yu, F. (2020b). Detecting and quantifying natural selection
550 at two linked loci from time series data of allele frequencies with forward-in-time simulations.
551 *Genetics*, *216*, 521–541.
- 552 He, Z., Dai, X., Beaumont, M. A., & Yu, F. (2020c). Estimation of natural selection and allele
553 age from time series allele frequency data using a novel likelihood-based approach. *Genetics*,
554 *216*, 463–480.
- 555 He, Z., Dai, X., Lyu, W., Beaumont, M. A., & Yu, F. (2022). Estimating and testing selection
556 and its changes from ancient DNA data. *bioRxiv*, (p. 502345).
- 557 Hunter, P. (2018). The genetics of domestication: Research into the domestication of livestock
558 and companion animals sheds light both on their “evolution” and human history. *EMBO*
559 *Reports*, *19*, 201–205.
- 560 Karlin, S., & Taylor, H. E. (1981). *A Second Course in Stochastic Processes*. New York:
561 Academic Press.
- 562 Larson, G., & Fuller, D. Q. (2014). The evolution of animal domestication. *Annual Review of*
563 *Ecology, Evolution, and Systematics*, *45*, 115–136.
- 564 Librado, P., Gamba, C., Gaunitz, C., Der Sarkissian, C., Pruvost, M. et al. (2017). Ancient
565 genomic changes associated with domestication of the horse. *Science*, *356*, 442–445.
- 566 Loog, L., Thomas, M. G., Barnett, R., Allen, R., Sykes, N. et al. (2017). Inferring allele
567 frequency trajectories from ancient DNA indicates that selection on a chicken gene coincided

- 568 with changes in medieval husbandry practices. *Molecular Biology and Evolution*, *34*, 1981–
569 1990.
- 570 Ludwig, A., Pruvost, M., Reissmann, M., Benecke, N., Brockmann, G. A. et al. (2009). Coat
571 color variation at the beginning of horse domestication. *Science*, *324*, 485–485.
- 572 Luengo, D., Martino, L., Bugallo, M., Elvira, V., & Särkkä, S. (2020). A survey of Monte Carlo
573 methods for parameter estimation. *EURASIP Journal on Advances in Signal Processing*,
574 *2020*, 1–62.
- 575 Lyu, W., Dai, X., Beaumont, M. A., Yu, F., & He, Z. (2022). Inferring the timing and strength
576 of natural selection and gene migration in the evolution of chicken from ancient DNA data.
577 *Molecular Ecology Resources*, *22*, 1362–1379.
- 578 Malaspinas, A.-S. (2016). Methods to characterize selective sweeps using time serial samples:
579 an ancient DNA perspective. *Molecular Ecology*, *25*, 24–41.
- 580 Malaspinas, A.-S., Malaspinas, O., Evans, S. N., & Slatkin, M. (2012). Estimating allele age
581 and selection coefficient from time-serial data. *Genetics*, *192*, 599–607.
- 582 Mathieson, I. (2020). Estimating time-varying selection coefficients from time series data of
583 allele frequencies. *bioRxiv*, (p. 387761).
- 584 Mathieson, I., Lazaridis, I., Rohland, N., Mallick, S., Patterson, N. et al. (2015). Genome-wide
585 patterns of selection in 230 ancient Eurasians. *Nature*, *528*, 499–503.
- 586 Pruvost, M., Bellone, R., Benecke, N., Sandoval-Castellanos, E., Cieslak, M. et al. (2011).
587 Genotypes of predomestic horses match phenotypes painted in Paleolithic works of cave art.
588 *Proceedings of the National Academy of Sciences*, *108*, 18626–18630.
- 589 Ramos-Madrigal, J., Smith, B. D., Moreno-Mayar, J. V., Gopalakrishnan, S., Ross-Ibarra, J.
590 et al. (2016). Genome sequence of a 5,310-year-old maize cob provides insights into the early
591 stages of maize domestication. *Current Biology*, *26*, 3195–3201.
- 592 Rieder, S., Taourit, S., Mariat, D., Langlois, B., & Guérin, G. (2001). Mutations in the agouti
593 (*ASIP*), the extension (*MC1R*), and the brown (*TYRP1*) loci and their association to coat
594 color phenotypes in horses (*Equus caballus*). *Mammalian Genome*, *12*, 450–455.

595 Roberts, G. O., & Rosenthal, J. S. (2001). Optimal scaling for various Metropolis-Hastings
596 algorithms. *Statistical Science*, *16*, 351–367.

597 Schraiber, J. G., Evans, S. N., & Slatkin, M. (2016). Bayesian inference of natural selection
598 from allele frequency time series. *Genetics*, *203*, 493–511.

599 Shim, H., Laurent, S., Matuszewski, S., Foll, M., & Jensen, J. D. (2016). Detecting and
600 quantifying changing selection intensities from time-sampled polymorphism data. *G3: Genes,*
601 *Genomes, Genetics*, *6*, 893–904.

602 Steinrücken, M., Bhaskar, A., & Song, Y. S. (2014). A novel spectral method for inferring
603 general diploid selection from time series genetic data. *The Annals of Applied Statistics*, *8*,
604 2203–2222.

605 Tataru, P., Simonsen, M., Bataillon, T., & Hobolth, A. (2017). Statistical inference in the
606 Wright-Fisher model using allele frequency data. *Systematic Biology*, *66*, e30–e46.

607 Terhorst, J., Schlötterer, C., & Song, Y. S. (2015). Multi-locus analysis of genomic time series
608 data from experimental evolution. *PLoS Genetics*, *11*, e1005069.

609 Vihola, M. (2012). Robust adaptive Metropolis algorithm with coerced acceptance rate. *Statis-*
610 *tics and Computing*, *22*, 997–1008.

611 Williamson, E. G., & Slatkin, M. (1999). Using maximum likelihood to estimate population
612 size from temporal changes in allele frequencies. *Genetics*, *152*, 755–761.

613 Wright, S. (1931). Evolution in Mendelian populations. *Genetics*, *16*, 97–159.

614 Wutke, S., Benecke, N., Sandoval-Castellanos, E., Döhle, H.-J., Friederich, S. et al. (2016).
615 Spotted phenotypes in horses lost attractiveness in the Middle Ages. *Scientific Reports*, *6*,
616 38548.

617 **Data Accessibility Statement**

618 The authors state that all data necessary for confirming the conclusions of the present work
619 are represented completely within the article. Source code implementing the adaptive version of

620 the PMMH algorithm described in this work is available at [https://github.com/zhangyi-he/](https://github.com/zhangyi-he/WFM-2L-DiffusApprox-AdaptPMMH/)
621 [WFM-2L-DiffusApprox-AdaptPMMH/](https://github.com/zhangyi-he/WFM-2L-DiffusApprox-AdaptPMMH/), where the standard version of the PMMH algorithm is also
622 available.

623 **Author Contributions**

624 Z.H. designed the project and developed the method; Z.H., X.D. and W.L. implemented the
625 method; X.D. and W.L. analysed the data under the supervision of Z.H., M.B. and F.Y.; Z.H.
626 wrote the manuscript; X.D., W.L., M.B. and F.Y. reviewed the manuscript.